The International Journal of Advanced Manufacturing Technology
https://doi.org/10.1007/s00170-026-18375-0

ORIGINAL ARTICLE

Solid-state recycling of pure aluminum chips via direct hot rolling: mechanical, microstructural, and corrosion insights

Mauro Carta[1] · **Pasquale Buonadonna**[1] · **Mohamad El Mehtedi**[1]

Received: 17 July 2025 / Accepted: 19 May 2026

Abstract
This study presents a novel method for recycling aluminum chips through direct hot rolling, eliminating the need for conventional melting processes. The solid-state recycling (SSR) approach reduces energy consumption, minimizes material loss, and mitigates environmental impact. Chips of pure aluminum (99.9wt.%) produced by turning were compacted, heat treated and subjected to hot rolling. Both compacted chips and parent-bulk material underwent the same rolling schedule achieving the final thickness of 0.8 mm. The produced sheets were subjected to microhardness, tensile tests, microstructure analysis (optical and SEM-EBSD techniques), density measurements, and corrosion tests. The recycled sheets exhibited average mechanical properties close to those of the parent-bulk material, albeit with higher data dispersion, with an Ultimate Tensile Strength (UTS) of 94.6 vs. 94.4 MPa, elongation at fracture (A%) of 7.0 compared to 7.1%, microhardness of 26.2 vs. 28.4 HV respectively, and lower corrosion rate for recycled chips. Overall, the results demonstrate the fundamental feasibility of direct hot rolling as a solid-state recycling route for pure aluminum chips under controlled conditions.

Keywords Pure Aluminum · Sustainable processes · Solid-State Recycling · Direct Hot Rolling · Mechanical testing

1 Introduction

Aluminum is one of the most widely used metals in industrial applications due to its excellent mechanical properties, low density, high corrosion resistance, and superior recyclability. Recycling aluminum saves up to 95% of the energy required for primary production, making it a keystone of circular economic strategies. However, based on remelting scrap, conventional recycling methods incur significant energy costs and material losses due to oxidation and dross formation [1].

Solid-state recycling (SSR) has emerged as a promising alternative, consolidating aluminum chips into bulk material without melting. Existing SSR methods, such as extrusion [2], ECAP [3], friction stir processing [4], friction stir consolidation [5], or spark plasma sintering [6], often need specialized equipment or additional preprocessing steps, complicating industrial scalability for large production. Even so, some attempts to scale SSR to industrial scale has been made [7]. Direct integration of SSR into established manufacturing workflows remains a critical challenge, particularly for high-volume applications like sheet production.

Among the various SSR techniques, direct hot rolling of compacted aluminum chips presents a promising approach for producing high-quality aluminum sheets without the need for melting [8]. This method is more energy-efficient than traditional aluminum recycling routes, as it avoids the melting step. Furthermore, it minimizes material loss and mitigates environmental impact [9, 10]. Direct hot rolling has been shown to effectively bond chip interfaces and produce consolidated sheets with mechanical properties comparable to wrought material in alloys such as AA3105 [11]. Moreover, combinations of direct rolling and severe plastic deformation techniques such as accumulative roll bonding (ARB) have demonstrated enhanced microstructural refinement and mechanical performance [12].

This study investigates the feasibility and effectiveness of direct hot rolling for recycling pure aluminum (AA1099) chips, focusing on the mechanical, microstructural, and corrosion properties of the recycled sheets. The use of

✉ Mauro Carta
mauro.carta94@unica.it

[1] Department of Mechanical, Chemical and Materials Engineering, University of Cagliari, Via Marengo 2, Cagliari 09123, Italy

Published online: 27 May 2026

ultra-high purity aluminum (AA1099) is intended as a controlled and simplified model system to verify the fundamental consolidation mechanism of direct hot rolling under ideal, uncontaminated conditions. Therefore, the present work should not be interpreted as a direct demonstration of industrial-grade chip recycling, where machining swarf typically contains lubricants, surface contaminants, alloying elements, and heterogeneous oxide layers. Instead, this study aims to isolate the intrinsic bonding and consolidation behavior of pure aluminum chips during direct hot rolling. The objective of this research is to assess whether the mechanical performance of the recycled material is comparable to that of bulk aluminum processed under similar conditions. The study evaluates key mechanical properties such as tensile strength, microhardness, and elongation, alongside microstructural analysis using optical microscopy and scanning electron microscopy (SEM-EBSD). Additionally, corrosion resistance is examined through potentiodynamic polarization tests to determine the long-term stability of the recycled aluminum in chloride environments.

2 Materials and methods

2.1 Recycling process: the direct hot rolling method

Aluminum chips (AA1099) were prepared. The machining process was carried out without the usage of lubricants, by turning a bar of high purity aluminum (99.99 wt%). Then, chips were cold compacted with an applied load of 150 kN with servo-hydraulic universal testing machine (MTS Systems Corporation, USA). Since the dimensions of compacted chips are estimated in cylinders of 40 mm of diameter and 9 mm height (Fig. 1b) the compacting pressure is around 120 MPa. Compacting pressure was chosen to obtain a relative density of around 80% and to make the chips handleable for subsequent operations [13]. The as received bar was characterized by 80 MPa UTS and 38% elongation according to the manufacturer.

All samples were heat treated for 2 h at 400 °C in a muffle furnace in ambient air, then hot rolled (HR) with several consecutive passes with the BW200 "Carl wezel, Mühlacker" at the rotation speed of 52 rpm with rolls diameter of 130 mm.

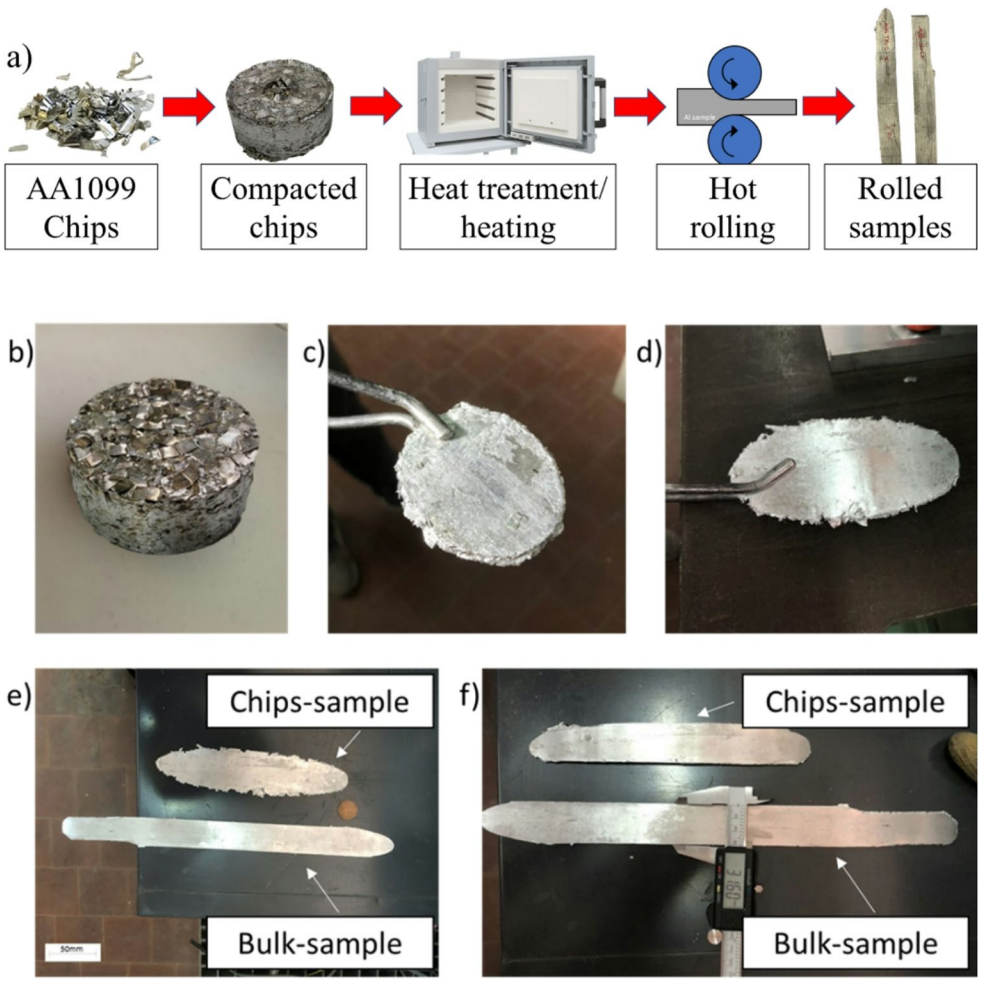

Fig. 1 (**a**) Schematic representation of the direct hot rolling recycling process; (**b**) compacted aluminum chips prior to rolling; (**c**) chips-based sample after the 1 st rolling pass; (**d**) chip-based sample after the 3rd rolling pass; (**e**) chip-based and bulk samples after the final rolling pass; (**f**) comparison of the two samples after trimming the irregular edges

The samples were heat treated and heated before hot rolling using a Nabertherm N50 muffle furnace. The selected heat treatment temperature and duration were not intended to define an optimized processing condition, but rather to provide a representative and conservative parameter set suitable for solid-state recycling via thermomechanical consolidation. In particular, annealing temperatures around 400 °C have been widely reported as critical for promoting recrystallization in high-purity aluminum after severe plastic deformation, while avoiding excessive grain growth [14, 15].

Compacted chips and bulk-material underwent similar rolling passes reported in Table 1. The chosen rolling schedule was kept as close as possible to that of industrial rolling passes. To restore the initial temperature of 400 °C after each rolling, samples were returned to the furnace for 10 min. The temperature of the rolls was kept at room temperature. After the last HR pass (7th pass), samples were fast cooled to room temperature. Finally, one last pass at room temperature (Cold rolling - CR) was carried out on every sample to reach the final thickness of 0.8 mm. This approach, commonly adopted in industrial rolling routes, allows improved dimensional accuracy and surface finish, while enhancing mechanical properties through work hardening and increased dislocation density [16]. Table 1 reported nominal thickness for every pass. Figures 1b-d show the samples during the rolling process.

In Fig. 1.e is shown one recycled-chips sample and a bulk-material sample. The chip-derived sheets exhibited jagged and sawtooth-like edges after multi-pass rolling, as shown in Fig. 1.f, leading to material losses during trimming. It should be noted, however, that edge trimming is a standard and unavoidable operation also in conventional rolling processes for aluminum sheets.

During the rolling experiments, key process parameters such as roll surface condition, roll temperature, and rolling speed were intentionally kept constant in order to isolate the effect of the recycling route itself. The rolls were maintained at room temperature and operated at a fixed rotational speed of 52 rpm, consistent with laboratory-scale rolling conditions and previous studies on direct hot rolling of aluminum chips [11, 12].

Although parameters such as friction coefficient, roll temperature, and rolling speed are known to influence metal flow, rolling force, and recrystallization behavior, a systematic sensitivity analysis was beyond the scope of the present feasibility-oriented study. However, to provide a quantitative description of the rolling process, the main process parameters, including thickness reduction, rolling force, torque, and power requirements, were estimated using classical rolling theory. These calculations are intended to provide an order-of-magnitude assessment of the process mechanics rather than a full thermo-mechanical modeling and were evaluated according to [17, 18].

Table 2 summarizes the estimated mechanical parameters associated with each rolling pass of the bulk reference material. For each pass, the thickness reduction and the corresponding true strain were first determined as:

$$\epsilon = \ln\left(\frac{h_0}{h_f}\right) \tag{1}$$

The strain rate was estimated from the roll kinematics as:

$$\dot{\epsilon} = \frac{2}{\sqrt{3}}\frac{v}{L_c}\ln\left(\frac{h_0}{h_f}\right) \tag{2}$$

where v is the roll peripheral speed and $L_c = \sqrt{R(h_0 - h_f)}$ is the roll–strip contact length.

The flow stress was then evaluated using a Hensel–Spittel constitutive equation [17], expressed as a function of strain, strain rate, and temperature. Based on the resulting flow stress, the roll force per unit strip width was calculated as:

$$F = P_m L_c \tag{3}$$

where P_m is the mean pressure on the rolls calculated based on Orowan-Pascoe theory. The rolling torque per roll and per unit width was determined using:

$$\mathrm{M_t} = F\lambda L_c \tag{4}$$

where λ is an experimentally determined coefficient, dependent on the rolling regime (0.5 for Hot Rolling and 0.4 for Cold Rolling).

Since the experimental rolling mill is equipped with two mechanically coupled rolls driven by a single motor, the total rolling torque was obtained by summing the contribution of both rolls. The rolling power per unit width was then calculated as:

$$W = 2\mathrm{M_t}\omega \tag{5}$$

Table 1 Rolling schedules adopted for bulk AA1099 and compacted chips. hx indicates the nominal thickness after the "x-th" rolling pass. Passes h0 to h7 correspond to hot rolling (HR), while h8 represents the final cold rolling (CR) pass

N. of passes	h0	h1	h2	h3	h4	h5	h6	h7	h8 (CR)
Bulk [mm]	10	8	6.5	5	4	2.5	1.75	1.25	0.8
Chips [mm]			9	5	4	2.5	1.75	1.25	0.8

Table 2 Bulk AA1050 rolling schedule results. For each rolling pass, the table reports thickness reduction Δh, true strain $\epsilon = \ln(h_{in}/h_{out})$, rolling force per unit width (N/mm), rolling torque per unit width, and total power per unit width (kW/m). Passes 1–7 correspond to hot rolling (HR), while pass 8 corresponds to the final cold rolling (CR) step. Torque and power are reported as total values for the two-roll mill (single motor with geared rolls)

Rolling regime	Rolling Pass	Thickness reduction (mm)	True strain (mm/mm)	Rolling force (*N*/mm)	Rolling torque (*N*·m/mm)	Rolling power (W/mm)
HR	1	2	0.22	676	2.7	29.4
HR	2	1.5	0.21	598	2.1	22.5
HR	3	1.5	0.26	656	2.3	24.7
HR	4	1	0.22	540	1.5	16.6
HR	5	1.5	0.47	910	3.1	34.2
HR	6	0.75	0.36	647	1.6	17.2
HR	7	0.5	0.34	570	1.1	12.4
CR	8	0.45	0.45	2039	3.9	42.0

where $\omega = 2\pi N/60$ is the angular velocity of the rolls and N is the roll rotational speed. For each pass, the thickness reduction, corresponding true strain, rolling force, torque, and power requirements are reported on a per-unit-width basis, allowing a consistent comparison across the rolling schedule. Passes 1–7 correspond to hot rolling (HR), where deformation is assisted by elevated temperature, while pass 8 represents the final cold rolling (CR) step carried out at ambient temperature. Results are shown in Table 2.

2.2 Material characterization

To assess the efficiency of the direct rolling process for recycling, each sample was analyzed in terms of mechanical properties, microstructure, density, and corrosion resistance. These tests were chosen to assess the mechanical strength and environmental durability of the recycled material.

The density of the samples was determined according to the well-known Archimedes principle by immersion in distilled water [19], providing a macroscopic evaluation of bulk density and overall densification. Mechanical properties were evaluated through tensile testing and Vickers microhardness measurements. Microstructural characterization was performed using optical microscopy, scanning electron microscopy (SEM), and electron backscatter diffraction (EBSD). Corrosion behavior was assessed using potentiodynamic polarization tests. All these tests were conducted exclusively on the fully rolled sheets. The compacted and heat-treated chip preforms were not mechanically tested, as they were intermediate states prior to rolling and not representative of the final consolidated material.

Tensile testing was conducted on all hot rolled sheets. At least five tensile specimens were machined from both recycled chip and bulk material conditions, along with rolling direction (RD). Testing followed the ASTM E8/E8M and BS EN 895 standards and was performed using a Galdabini SUN500 electromechanical universal testing machine with a maximum axial load capacity of 5 kN.

Vickers microhardness measurements were performed in accordance with ASTM E-384. For each material condition, a minimum of six Vickers microhardness indentations were performed on the transverse section at half of the sheet thickness, with the indents aligned along the rolling direction (RD). Prior to testing, sample surfaces were ground to a 2500-grit. Measurements were carried out using an EmcoTest M1C010 microhardness tester.

To further assess the surface quality of the rolled sheets, areal surface roughness (Sa) were measured on both bulk and recycled chip-based AA1099 samples in the as-rolled condition. Measurements were performed using a Keyence VHX-X1 digital microscope equipped with 3D surface reconstruction capability on representative areas to evaluate potential topographical differences induced by the chip-based feedstock.

Microstructural analysis was conducted on both bulk and chip-derived samples using an Olympus BX53M in polarized light microscope. Standard metallographic preparation techniques were employed, including cutting, resin mounting, grinding to a 2500-grit finish, and polishing with a 3 µm diamond suspension followed by a 0.25 µm colloidal silica (OP-S) solution. Samples were etched with Barker's reagent (5% HBF_4) using a Struers Lectropol-5 at 20 V and examined under polarized light to reveal the grain structure.

For SEM analysis, samples were mechanically polished, while for EBSD measurements, an additional electropolishing step was required to eliminate surface deformation and scratches. The last was performed using Struers Lectropol-5 with Struers AC2 electrolyte at 20 V for 20 s. The SEM/EBSD characterization was conducted using a Zeiss Ultra 55 Gemini FEG-SEM.

2.3 Corrosion tests

To investigate the corrosion behavior of both recycled-chip and bulk material samples, potentiodynamic polarization

tests were conducted at room temperature in a neutral 3.5% NaCl aqueous solution. All samples were tested in as-rolled condition, with at least three repetitions performed for each condition.

Sample preparation involved cutting specimens to 15×15 mm^2 dimensions, grinding them to a 2500-grit finish, and then cleaning with ethanol. This procedure was implemented to remove potential iron contamination from the rolling process, which could act as cathodic sites and accelerate galvanic corrosion in aluminum, thereby ensuring uniform and reliable surface conditions for accurate corrosion measurement. The tests were conducted in a standard setup with 3-electrode within a plexiglass cell.

Throughout the experimentation, a stirrer was employed to maintain solution consistency. Samples were fixed to a cell with a 0.5 cm^2 opening, ensuring a constant exposed surface area. Each sample was mounted in the cell using an O-ring and a screw to ensure both a seal and electrical contact, with a defined exposed area of 0.5 cm². After filling the cell with the NaCl solution, any air bubbles formed on the sample surface were removed using a pipette. Figure 2.a depicts a picture of the actual experimental setup, while Fig. 2.b provides a schematic representation. Finally, the counter and reference electrodes were introduced into the cell to proceed with the analysis.

As already mentioned, the experimental setup consists of electrical connection (Fig. 2.b) of 3 fundamental elements to the potentiostat:

- the counter electrode (CE), consisting in a platinum grid;
- the working electrode (WE), the sample under test;
- The reference electrode (RE), a standard electrode with silver chloride (Ag | AgCl | sat 3.5 M KCl): the commercial name is HI5311 by Hanna Instruments.

Every polarization test lasts approximately 90 min and was repeated at least three times for each condition.

During this process, the potentiostat measures the potential difference between the working electrode (WE) and the reference electrode (RE). The RE maintains a fixed and known potential as no current flows through it. Throughout the test, the applied potential at the WE is increased linearly at a scan rate of 12 mV per minute, based on the software inputs.

The software generates a graph from the test data, enabling users to determine the potential values and key current densities. All tests are conducted at room temperature.

Electrochemical impedance spectroscopy (EIS) measurements were carried out using a conventional three-electrode cell, with the sample that serves as working electrode, while a platinum grid and a saturated calomel electrode (SCE) were used as counter and reference electrode, respectively. The tests were performed in 35 g/L NaCl solution at room temperature under open circuit potential (OCP) conditions after 0, 24 and 72 h of immersion. A sinusoidal perturbation amplitude of 10 mV was applied over the 100 kHz-10 mHz frequency range to ensure a linear system response during EIS measurements. This frequency range allowed the characterization of both passive film properties and interfacial charge-transfer processes.

3 Results and discussion

3.1 Microstructure characterization

Figures 3.a-b show the microstructures of the bulk-samples, showing typical microstructure of hot rolled alloy. Elongated grains aligned with the Rolling Direction (RD) are visible in Fig. 3.a, while Fig. 3.b shows rounded-shape grains perpendicular to the RD. The bulk material's microstructure suggests that recovery, rather than full recrystallization, occurred during hot rolling. This process was accompanied by significant grain growth, which is a

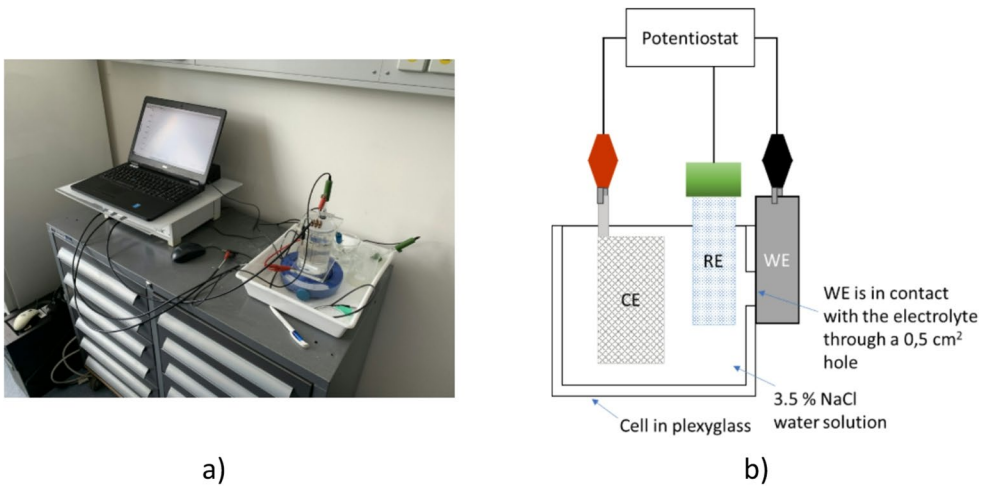

Fig. 2 (**a**) Experimental setup used for the potentiodynamic polarization tests; (**b**) of the electrochemical cell, highlighting the electrical connections between working, reference, and counter electrodes

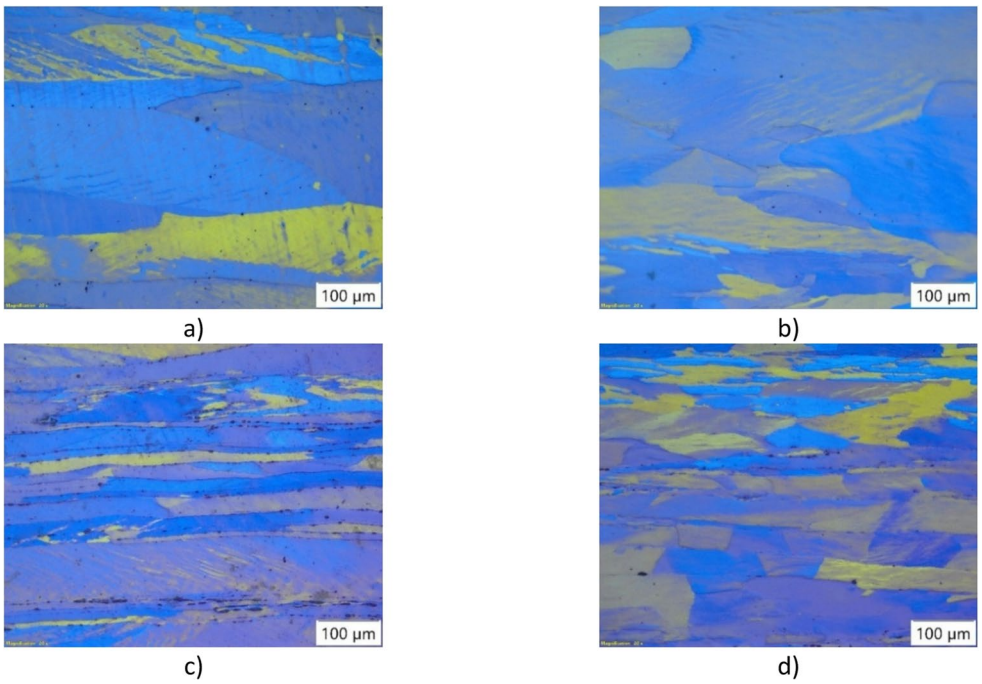

Fig. 3 (**a**) Optical micrograph of the bulk AA1099 sample parallel to the rolling direction (RD); (**b**) cross-sectional micrograph of the bulk sample; (**c**) optical micrograph of the recycled chip-based sample parallel to RD; (**d**) cross-sectional micrograph of the recycled chip-based sample

characteristic of high-purity aluminum [20]. Figures 3.c-d show the microstructures of the recycled-chip samples. Figure 3.c reveals an elongated and layered structure along the Rolling Directions, whereas Fig. 3.d shows a layered structure with finer grains. Optical microscopy was used primarily to assess overall microstructural integrity and identify macroscopic defects. At the magnifications employed, both materials appeared fully consolidated on the optical scale. For a higher-resolution investigation of local interfaces and defects, field-emission scanning electron microscopy (FE-SEM) coupled with EDS analysis was used, as detailed in Sect. 3.3. This microstructural configuration is consistent with partial recrystallization occurring during hot rolling, confirming the effectiveness of the rolling process in producing continuous sheets.

The EBSD measurements were carried out on a transversal section at the mid-thickness of each sample. The measured area is 250×350 µm^2 with a 0.4 µm step size.

The black lines in Fig. 4.a and Fig. 4.b indicate high-angle grain boundaries (HAGBs), defined by misorientation angles greater than 15°.

The EBSD measurements confirmed what was already observed in the optical micrographs and provided deeper information on the microstructures.

Figure 4.a exhibits relatively large and slide elongated grains with an average grain diameter ($\bar{d}_g$) of approximately 203 µm, together with a broad distribution of crystallographic orientations. This microstructure is characteristic of a material that has not undergone substantial recrystallization during hot rolling and is consistent with previous studies on high-purity aluminum, where recrystallization readily occurs once sufficient thermal activation and plastic strain are provided, after annealing [20].

In contrast, the recycled chip-based AA1099 sample (Fig. 4.b) displays a more layered and striated pattern. The IPF map reveals a pronounced layered and elongated grain structure aligned along the rolling direction (RD), with a significantly smaller average grain size of approximately 59 µm. The increased orientation alignment and lamellar morphology are attributed to the constraining influence of the original chip boundaries, with a larger fraction of deformation-induced substructures retained after rolling.

The misorientation angle distributions shown in Figs. 4.c-d further clarify these differences. In the bulk material, the distribution is dominated by low-angle grain boundaries (LAGBs, 3–15°), with a rapid decrease in frequency at higher misorientation angles, resulting in a HAGB fraction of approximately 41.3%. This distribution reflects an incomplete recrystallization process, where recovery mechanisms like subgrains coalescence have occurred, but full boundary migration and grain growth have been suppressed.

In the AA1099 recycled-chips sample, like that of the bulk material, there is a concentration of boundaries at lower misorientation angles. The distribution pattern is quite similar, with the major peak also around 3 degrees. It also shows a decrease in number fraction as the angle increases, albeit the decrease is not as steep as in the bulk sample and with a smaller peak for high angle boundaries around 50°.

Despite both samples being hot rolled with the same schedule, the microstructure of the chip-based material shows signs of more retained deformation compared to the bulk. This contrast can be partly explained by the

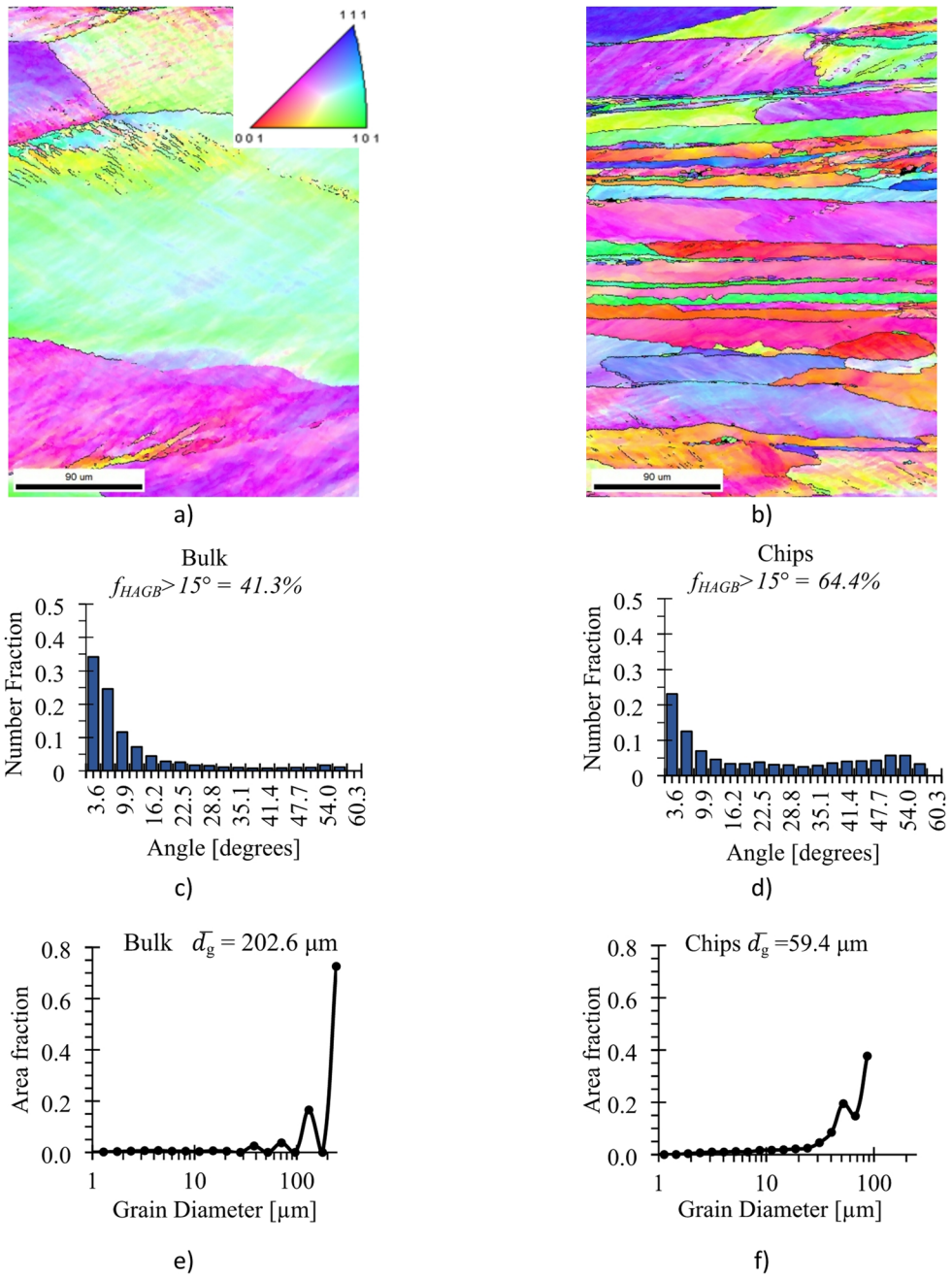

Fig. 4 Inverse pole figure (IPF) maps of AA1099: (**a**) bulk material and (**b**) recycled chip-based sample; corresponding misorientation angle distributions for (**c**) bulk material and (**d**) recycled chips (high-angle grain boundaries (misorientation > 15°) are highlighted); grain diameter distributions for (**e**) bulk material and (**f**) recycled chip-based sample, with average grain diameters indicated. The rolling direction (RD) is aligned with the scale bars

intrinsic recrystallization behavior of high-purity aluminum. In ultra-high-purity aluminum such as AA1099, static recrystallization readily occurs at relatively low strains and temperatures but is often rapidly followed by pronounced grain growth due to the absence of solute drag and effective pinning mechanisms, resulting in coarse-grained microstructure observed in the bulk material [20]. In the recycled chip-based material, on the other hand, the compacted chip experiences stronger local strain gradients and pronounced strain partitioning during the early rolling passes. Such heterogeneous deformation can stabilize deformation-induced substructures, thereby delaying the onset and progression of full recrystallization after deformation. In addition, the higher fraction of high-angle grain boundaries observed in the chip-based material may be associated with the presence of residual oxide fragments, originating from the chip surfaces, which locally limit recrystallization of the α-Al matrix [21]. Unlike conventional remelting-based recycling, where oxide films are largely removed into the dross phase [1], solid-state recycling routes retain these fragmented oxides within the material, leading to distinct microstructural evolution pathways during deformation-driven consolidation. The layered microstructure observed in the recycled chip-based AA1099 sheets, and the reduced

extent of recrystallization can be rationalized in the framework of classical grain boundary migration theories. During thermomechanical consolidation, residual oxide fragments originating from the chip surfaces are known to act as effective obstacles to grain boundary motion, exerting a pinning pressure that limits boundary migration and grain growth. According to Zener's theory [22, 23], a reduced particle size combined with an increased volume fraction of second-phase particles results in a higher pinning pressure on grain boundaries, that limits their migration during annealing. In the present system, fragmented oxide residues act as effective pinning centers, restricting recrystallization unless the pinning force is overcome.

One must consider that compacted chips experience stronger local strain gradients as well as strain partitioning during early passes, which can stabilize deformation substructures and delay the transition to a fully recrystallized state.

The effects of oxide particles in solid-state recycling of aluminum chips are widely reported in the literature, particularly for extrusion-based consolidation routes [2, 24]. In this context, the layered morphology observed via EBSD may be interpreted as the combined result of strain partitioning during rolling and locally constrained grain boundary mobility at former chip interfaces. Although no quantitative recrystallization kinetics or dislocation density calculations were performed in this study, the experimental observations are consistent with established metallurgical models describing particle-pinned grain boundary migration in aluminum systems.

3.2 Mechanical properties

Representative stress-strain curves for both bulk and recycled chip-based samples are reported in Fig. 5a. Data dispersion and repeatability are quantified by the standard deviations shown as error bars in Fig. 5b and c. The ultimate tensile stress (UTS) for the recycled chips is measured at 94.6 ± 10.5 MPa, while for the bulk material, it is slightly lower at 94.4 ± 5.3 MPa. Although the mean UTS values are very close, the recycled chip-based samples exhibit a higher standard deviation, indicating greater variability in mechanical response likely associated with microstructural inhomogeneities and local interfacial defects typical of solid-state chip consolidation.

Furthermore, the percentage elongation at fracture (A%) also presents a close match between the two materials. The recycled chips have a recorded A% of 7.0 ± 0.6%, while the bulk material manifests a marginally higher value of 7.1 ± 0.3%. Again, the proximity in these values underscores the analogous ductile response of both materials under tensile loading. The Vickers Hardness of the bulk material (28.4 ± 1.3) is slightly harder than the chips (26.2 ± 1.2), as indicated in Table 3, though the difference lies within the range of measurement errors. The similar stress-strain behavior and low elongation (~7%) for both materials (Fig. 5a) indicate that the mechanical response is dominated by the work hardening introduced during rolling, which significantly reduces ductility from the original as-received bulk material (38% elongation). The fact that the recycled chips achieve comparable plasticity despite initial fragmentation and oxide presence suggests that effective metallurgical bonding was achieved during solid-state rolling consolidation.

Both materials show near-theoretical density values, with measured densities of 2.70 g/cm³ for the recycled chip-based samples and 2.69 g/cm³ for the bulk material, almost identical to the nominal density of pure aluminum, which is approximately 2.70 g/cm^3 [25]. This result indicates a high level of densification and negligible macroscopic porosity at the bulk scale. However, it should be noted that the Archimedes method is not sensitive to localized micro-porosity, and indeed FE-SEM observations revealed the presence of small, localized sub-micrometric voids at former chip interfaces, as discussed in Sect. 3.3, while no such defects were observable at the optical scale.

In summary, the average mechanical properties of the recycled chips are close to those of the bulk material, albeit with a noticeably higher data dispersion reflecting the intrinsic heterogeneity of the chip-derived microstructure. The increased scatter in the recycled samples is consistent with localized interfacial discontinuities and oxide-related features inherent to chip-based solid-state consolidation further discussed in the following paragraph 3.3.

3.3 Fracture surfaces, SEM and EDS analysis

Field-emission SEM observations were carried out to investigate fracture surfaces and local defects at chip interfaces, which are not reliably detectable by optical microscopy alone. Fig.7aa shows the energy-dispersive X-ray spectroscopy (EDS) analysis of one of the samples, confirming the high purity of the studied alloy. As expected for ultra-high-purity aluminum, no second-phase particles or inclusions were detected in the bulk material.

In contrast, localized sub-micrometric defects were observed in the recycled chip-based samples, as shown in Figs. 6b-c. Linear EDS measurements distinctly indicate a higher concentration of oxygen near the defect borders. This suggests that these defects originate from suboptimal bonding at former chip interfaces due to locally incomplete consolidation during solid-state processing. Due to its extremely small thickness, typically in the range of 2–10 nm, the native Al_2O_3 layer cannot be directly resolved at the

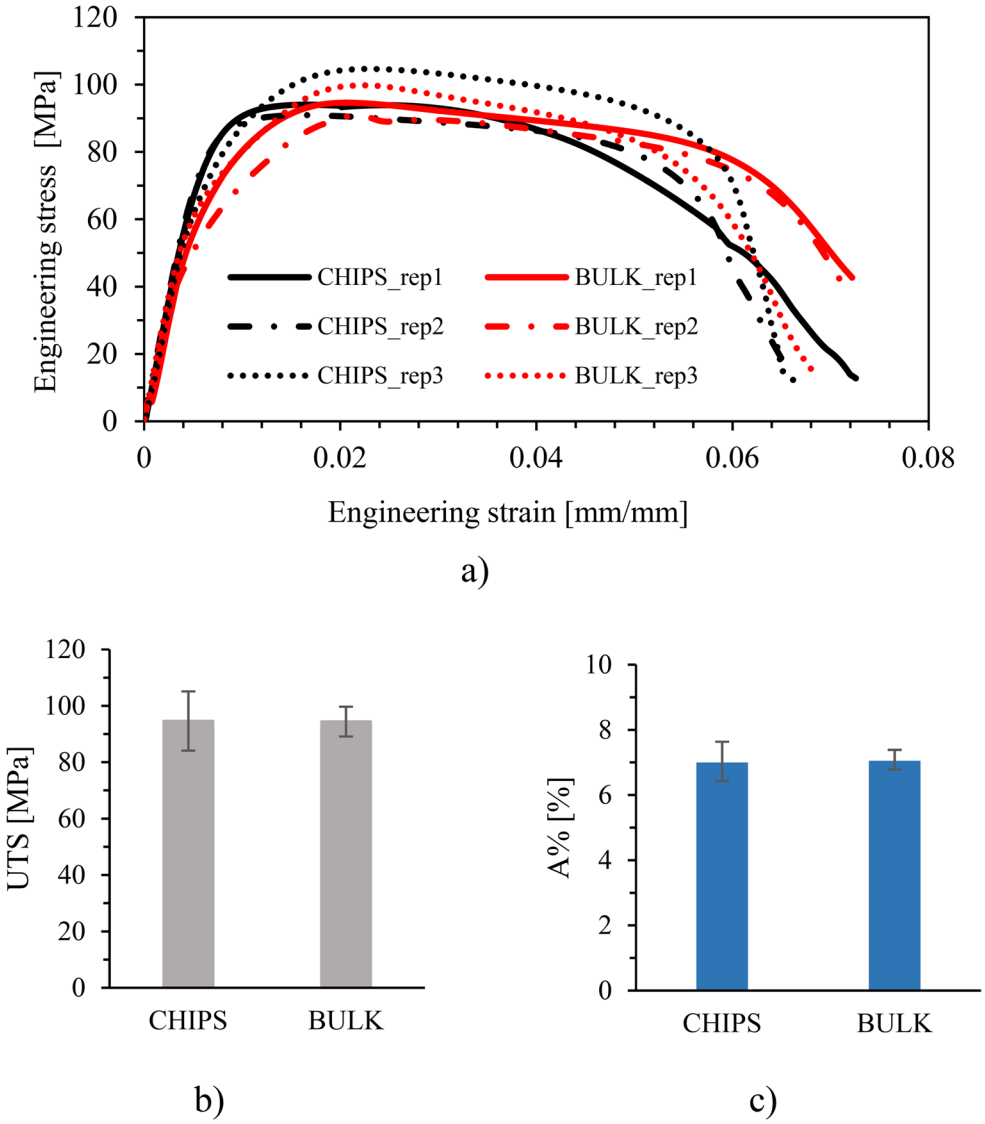

Fig. 5 (**a**) Representative engineering stress–strain curves of bulk and recycled chip-based AA1099 samples; comparison of (**b**) ultimate tensile strength (UTS) and (**c**) elongation at fracture (A%), with error bars indicating standard deviation

Table 3 Mechanical properties of recycled chips and bulk AA1099 samples after the rolling process

	UTS [MPa]	A% [%]	$HV_{0.2}$	Density [g/cm^3]
Chips	94.6 ± 10.5	7.0 ± 0.6	26.2 ± 1.2	2.70 ± 0.01
Bulk	94.4 ± 5.3	7.1 ± 0.3	28.4 ± 1.3	2.69 ± 0.01

magnifications available with the Zeiss 55 FE-SEM. Nevertheless, the localized oxygen enrichment detected by EDS provides indirect evidence of residual oxide-related features that may influence bonding quality and microstructural evolution in the recycled material.

The oxide-network model recently proposed for solid-state recycling of aluminum chips by Duchateau et al. [2, 24] can be conceptually adapted to the present direct hot rolling route. In the case of AA1099, the retained oxide is expected to consist mainly of fragmented Al_2O_3 films originating from the initial chip surfaces. During multi-pass rolling, these films are progressively fractured, elongated, and redistributed along former chip interfaces. Such oxide fragments may locally hinder grain-boundary migration and contribute to the finer and more layered microstructure observed in the recycled material. However, a quantitative description of this mechanism would require dedicated TEM-based statistical analysis, oxygen-content measurements, and surface-sensitive characterization techniques such as XPS, which are beyond the scope of the present study.

Fig7a-b are SEM micrographs revealing the morphology of the fracture surfaces for AA1099 in both bulk and chip forms, magnified at 1000×

The bulk material (Fig. 7a) exhibits a homogenous and continuous fracture surface characterized by smooth, wavy features and elongated shear markings. This morphology is indicative of a ductile fracture mechanism dominated by plastic flow, typical of ultra-high-purity aluminum where fracture occurs with limited microvoid nucleation due to the

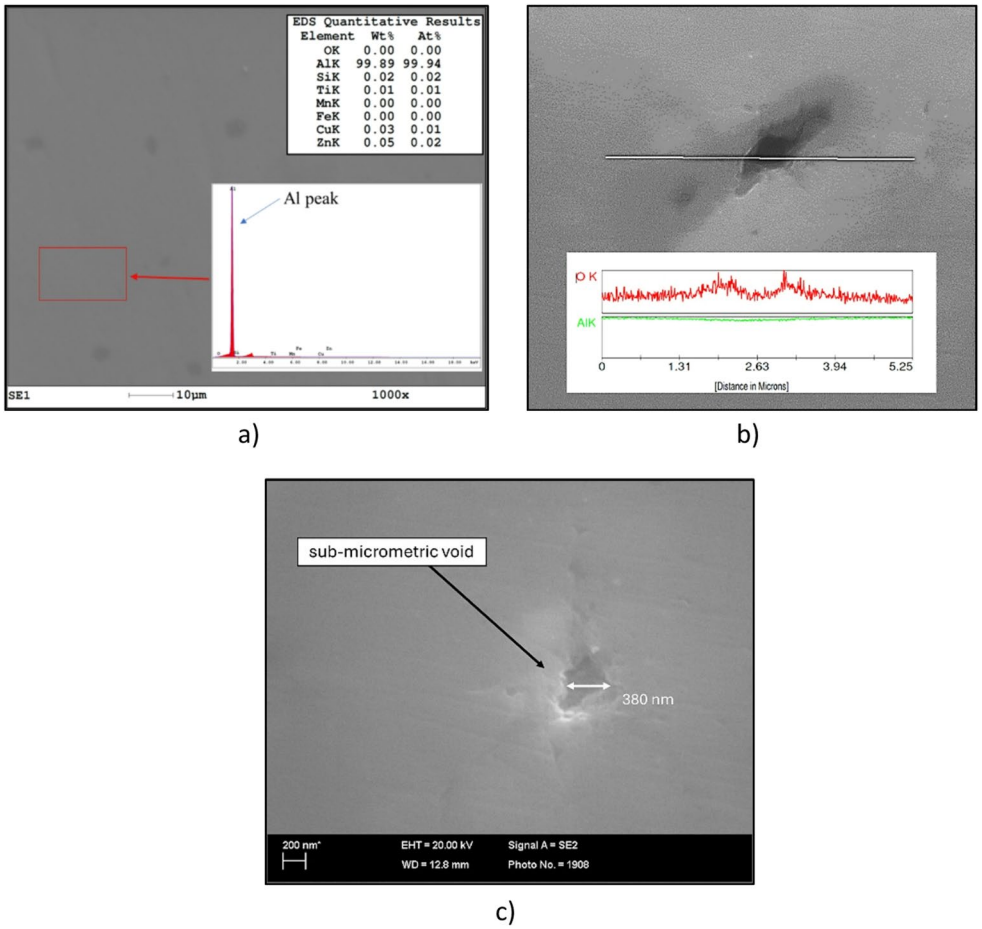

Fig. 6 (a) Energy-dispersive X-ray spectroscopy (EDS) analysis confirming the high purity of AA1099; (b) linear EDS scan across a defect in the recycled chip-based sample, showing localized oxygen enrichment associated with oxide layers; c) high-magnification FE-SEM micrograph showing a small, localized sub-micrometric void within the aluminum matrix.

absence of second-phase particles or inclusions. The lack of well-defined equiaxed dimples is consistent with the high purity of the material, as void nucleation sites are scarce, and plastic deformation is accommodated mainly through shear localization. In contrast, the chip-derived sample (Fig. 7b) displays a more heterogeneous fracture morphology, with a rougher surface characterized by numerous dimples and voids of varying size and shape. These features are characteristic of a ductile fracture mechanism governed by microvoid nucleation, growth, and coalescence. The presence of larger and irregular voids is attributed to former chip interfaces, where bonding may be locally incomplete due to residual oxide layers, as also evidenced by EDS analyses. These interfaces act as preferential void nucleation sites, resulting in localized stress concentrations during tensile loading. The fracture surface exhibits pronounced variations in texture and relief, reflecting the challenges in achieving uniform consolidation from chip-based material. Higher-magnification SEM images (3000×) shown in Fig. 7c and d further emphasize these differences. The bulk material (Fig. 7c) exhibits a more uniform fracture surface with elongated tearing ridges and limited cavity formation, confirming a homogeneous plastic deformation process. Conversely, the recycled chip-based sample (Fig. 7d) reveals well-developed dimples with pronounced depth and size variability, highlighting the influence of microstructural heterogeneities, such as residual oxide layers and prior chip boundaries, inherited from the consolidation process.

Figure 7e shows a photograph of the tensile specimens after testing. In both bulk and recycled materials, fracture occurs along a plane inclined at approximately 45° with respect to the loading direction, which is characteristic of shear-dominated ductile fracture. Despite the microstructural differences and the presence of oxide-related interfaces in the recycled material, the macroscopic fracture mode remains ductile for both conditions, in agreement with the comparable elongation values measured during tensile testing.

3.4 Surface quality and roughness

The surface quality of the as-rolled sheets was evaluated using a Keyence VHX-X1 digital microscope with 3D surface reconstruction capability, without any additional surface finishing. Representative surface micrographs of the bulk and recycled chip-based AA1099 sheets reveal

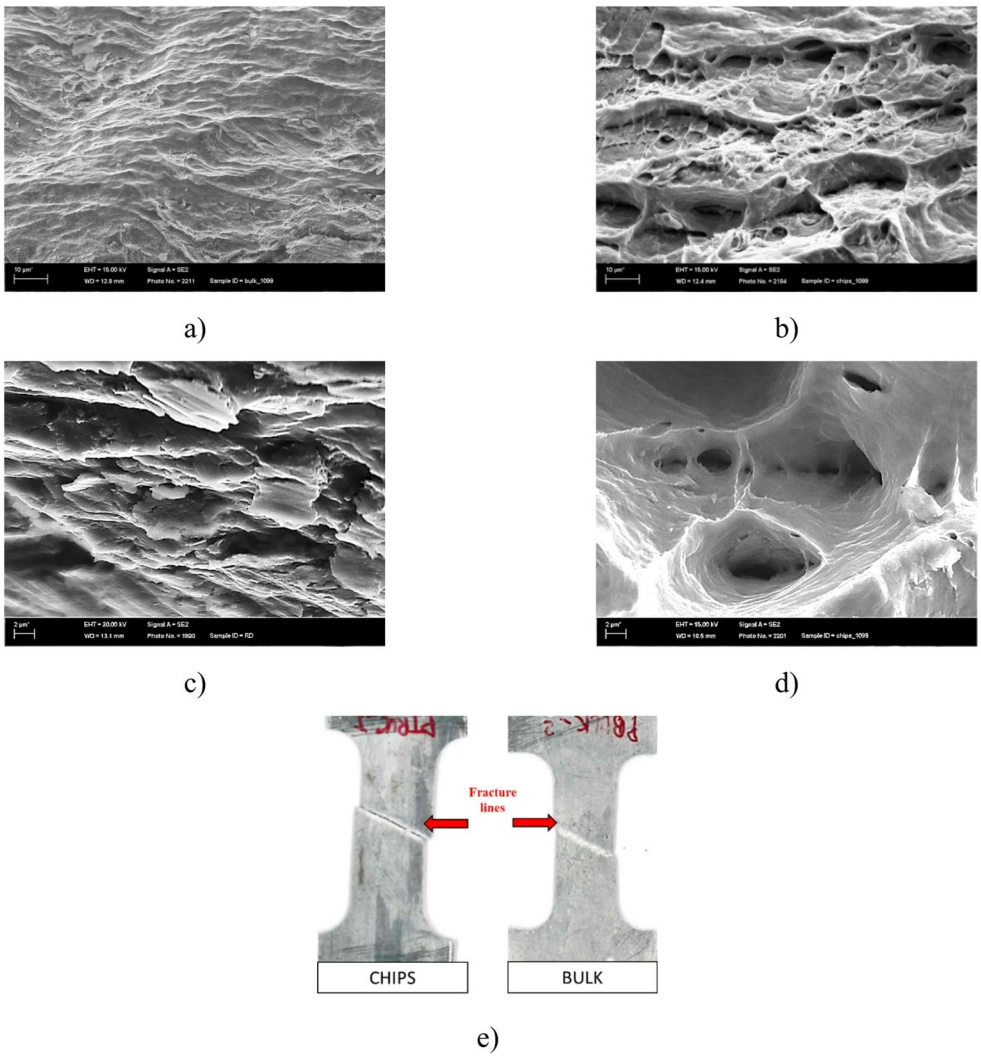

Fig. 7 SEM micrographs of the fracture surface of AA1099: (**a**) bulk material and (**b**) recycled chip-based sample (magnification 1,000×); higher-magnification SEM images (3000×) of the fracture surfaces for (**c**) bulk material and (**d**) recycled chip-based sample, highlighting the different fracture morphologies; (**e**) photographs of the tensile specimens after testing, showing the characteristic fracture angle of approximately 45° for both bulk and recycled materials

elongated surface features aligned along the rolling direction, reflecting the direct imprint of the rolling process on both materials (Fig. 8a and b). In both cases, the surface morphology is dominated by shallow grooves and flattened asperities, with no evidence of macroscopic surface defects such as cracks or delamination.

Quantitative roughness analysis over the entire areas shown in Figs. 8a and b shows that the bulk material exhibits a lower average areal roughness, with a measured Sa value of approximately 0.54 µm, whereas the recycled chip-based sample presents a moderately higher roughness, with Sa of 0.77 µm. This increase can be attributed to the heterogeneous deformation associated with the consolidation of chip interfaces and the presence of locally harder regions linked to residual oxide fragments. Nevertheless, the overall roughness levels remain within the same order of magnitude, indicating that direct hot rolling of aluminum chips does not lead to a severe degradation of surface quality compared to conventionally processed bulk material.

3.5 Corrosion tests: potentiodynamic polarization experiments

Potentiodynamic polarization tests are commonly used to assess the corrosion behavior of metals and alloys. These kinds of tests are important in manufacturing to evaluate how materials perform in real environmental conditions. They help ensure durability, reduce failure risks, and guide material selection for long-term applications. To perform a potentiodynamic polarization test, a working electrode made of the metal or alloy to study, a reference electrode (usually a saturated calomel electrode or a silver/silver chloride electrode), and a counter electrode (usually made of platinum), are all immersed in an electrolyte solution that simulates the environment in which the metal will be exposed. The setup consists of an electrochemical cell. The working electrode is the sample of interest while the reference electrode provides a stable reference potential, and the counter electrode completes the electrical circuit [26].

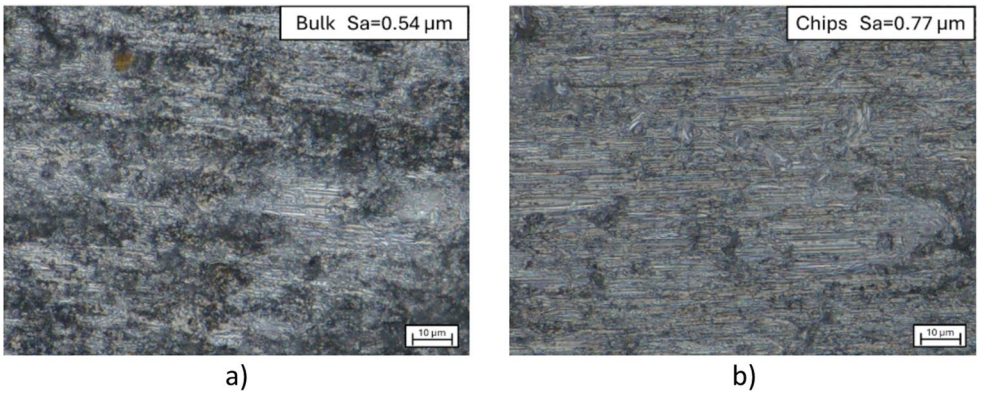

Fig. 8 Optical surface topography of AA1099 sheets in the as-rolled condition: (**a**) bulk material (Sa = 0.54 µm) and (**b**) recycled chip-based sample (Sa = 0.77 µm). Images acquired using a Keyence VHX-X1 digital microscope with 3D surface reconstruction; the rolling direction is aligned with the scale bar

In a potentiodynamic polarization test, the potential of the working electrode with respect to the reference electrode is varied over a range of values. This is done by sweeping the voltage at a controlled rate. As the potential changes, the current passing through the cell is measured. The current is a measure of the electrochemical reactions occurring at the metal's surface. Specifically, there is usually interest in both the anodic (oxidation) and cathodic (reduction) currents [27].

The data collected during the potential scan is processed to construct polarization curves that show the relationship between current and potential. The recorded data is usually presented on a voltage vs. logarithmic current graph. Figure 9 represents an example of ideal results from potentiodynamic tests.

By analyzing the polarization curves, several important parameters can be determined, including:

- corrosion potential (E_{corr}): the potential at which the anodic and cathodic currents are balanced, representing the corrosion tendency of the material;
- corrosion current density (i_{corr}): the rate at which the metal corrodes, calculated from the polarization curve;
- tafel slopes: β_a and β_c, known as anodic and cathodic Tafel slope, these slopes are used to estimate the rate of electrochemical reactions and can provide insights into the corrosion mechanism.

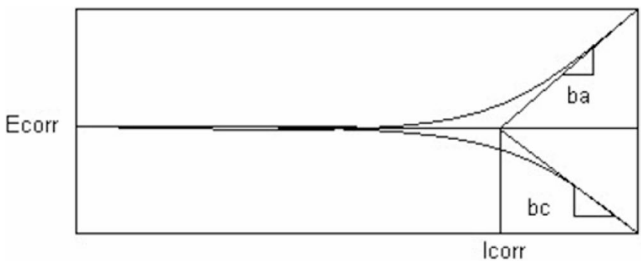

Fig. 9 Schematic example of a potentiodynamic polarization curve, showing electrode potential versus logarithmic current density [29]

These important parameters describe the carrion behavior of a metal. To determine the Tafel slopes, two tangents were drawn: one aligned with the predominant points on the cathodic curve for the βc value, and the other in line with the most common points on the anodic curve for the βa value. E_{corr} and i_{corr} values were derived from where these two tangents intersected [28] as shown in Fig. 9.

Sodium chloride (NaCl), used for all the corrosion tests described in this paragraph, is commonly used as an electrolyte solution in corrosion testing, because it represents a realistic environmental condition since sodium chloride is a common component of natural environments, especially in coastal and marine settings.

The cathodic reaction for aluminum in sodium chloride solution are [30, 31]:

$$O_2 + H_2O_{(s)} + e^- = OH^-_{ads} + OH^- \tag{6}$$

And:

$$OH_{ads} + e^- = OH^- \tag{7}$$

The anodic reaction instead happens on the surface of the aluminum alloy, such as:

$$Al_{(s)} + 3OH^- = Al(OH)_{3,ads} + 3e^- \tag{8}$$

$$Al\,(OH)_{3,ads} = Al_2O_3 \cdot 3H_2O \tag{9}$$

In summary, the test is executed applying a potential different from the equilibrium potential (E_{corr} to the working electrode (WE) using a potentiostat. This causes a flow of charges across the electrode interface. Current flows through the test solution and the counter electrode (CE) to the outside of the WE, and the software (Sequencer ®) provides the user with the current value. The Voltage and current obtained during the experiments are stored by the software allowing further data analysis.

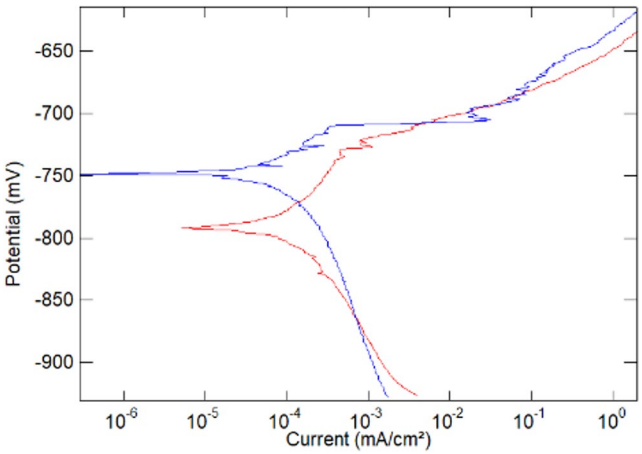

Fig. 10 Representative Tafel polarization curves of AA1099 bulk material (red curve) and recycled chip-based sample (blue curve) obtained in a 3.5 wt% NaCl solution

Analysis of the data. The important parameters β_a, β_c and i_{corr} can be derived from the plot as described before. The polarization resistance (R_p) was calculated using the well known Stern–Geary relationship [28]:

$$R_p = \frac{1}{i_{corr}} \left(\frac{\beta_a \beta_c}{2.3(\beta_a + \beta_c)} \right) \tag{10}$$

Where β_a and β_c are the Tafel slope, anodic and cathodic, respectively. R_p is inversely related to the rate of corrosion: higher Rp values signify lower corrosion rates.

The corrosion rates could be evaluated as (according to ASTM G102 standard):

$$K_{corr} = i_{corr} \left(\frac{K_1 E_w}{\rho} \right) \tag{11}$$

Where K_1 is a constant $3.27 \cdot 10^{-3}\, mm \cdot g \cdot (\mu A \cdot cm \cdot yr)^{-1}$, E_w is the equivalent weight of metal ($E_w = 8.99$ for aluminum) and ρ is the density of the metal ($\rho = 2.7 \frac{g}{cm^3}$).

The results presented in Fig. 10 showcase the potentiodynamic polarization test outcomes for both bulk materials and recycled chips of AA1099 tested in a 3.5% sodium chloride solution.

Table 4 summarizes several key parameters obtained from the polarization curves. The polarization resistance (Rp) values reported in Table 4 were calculated according to Eq. (10). The corrosion current density (Icorr) was obtained by Tafel extrapolation at the corrosion potential (Ecorr). The corrosion rate (Kcorr) was calculated following the ASTM G102 standard, using Eq. (11).

In the Handbook of aluminum [32] is reported a value of i_{corr} of 0.1 µA/cm2 for extreme purity aluminum under similar conditions, very close to the value obtain in this experiment (0.077 ± 0.02 µA/cm2), a confirmation of the validity of the results. Compared to the bulk material, the recycled chip-based AA1099 sample shows a slightly lower corrosion current density (0.05 ± 0.01) and a more noble corrosion potential. Consistently, the recycled material exhibits a marginally higher polarization resistance and a lower calculated corrosion rate, although the difference between the two conditions remains limited.

Rp, the polarization resistance, is inversely related to the corrosion rate: higher Rp values indicate lower corrosion rates. In this study, the AA1099 chips show a higher Rp than the bulk material, which is consistent with their lower i_{corr} value.

The slightly lower corrosion current density and the more noble corrosion potential observed for the recycled chip-based AA1099 sheets indicate that the direct hot rolling process does not degrade the corrosion performance. While these trends may be associated with differences in oxide film evolution during thermomechanical processing, the passive film characteristics were not directly measured in this study. Advanced surface-sensitive techniques such as X-ray photoelectron spectroscopy (XPS), electrochemical impedance spectroscopy (EIS), or Mott–Schottky analysis would provide further insight into the electronic structure and thickness of the passive film, the present study focuses on a comparative assessment of corrosion performance. Within this scope, the observed electrochemical behavior consistently indicates that the direct hot rolling recycling process does not degrade, and may slightly improve, the corrosion resistance of ultra-high purity aluminum.

The EIS spectra were fitted using the equivalent electrical circuit reported in Fig. 11, consisting of the solution resistance (Rs) and two R–CPE time constants associated with the passive oxide film and the charge-transfer process at the metal/electrolyte interface. Constant phase elements (CPEs) were used instead of ideal capacitors to account for the non-ideal capacitive behavior related to surface heterogeneity and interfacial inhomogeneity. The fitting parameters obtained for bulk and recycled-chip samples after 0, 24 and 72 h of immersion in 35 g/L NaCl are reported in Table 5.

Table 4 Corrosion parameters derived from potentiodynamic polarization curves of bulk and recycled chip-based AA1099 samples tested in a 3.5 wt% NaCl solution. Rp and Kcorr values were calculated according to the Stern–Geary relation and ASTM G102 standard, respectively

	E_{corr}(mV)	βa (mV)	βc (mV)	i_{corr} (µA·cm^{-2})	Rp (kΩ·cm²)	Kcorr (mm·year^{-1})
1099 bulk	−794±3	83±2	77±11	0.077±0.02	226.052	0.000835
1099 chips	−755±9	49±11	57±13	0.050±0.01	229.608	0.000549

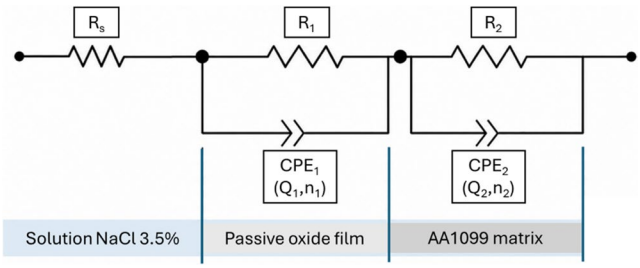

Fig. 11 Equivalent electrical circuit used to fit the EIS spectra of bulk AA1099 and recycled-chip samples immersed in 35 g/L NaCl solution. Rs represents the solution resistance, while the two R–CPE time constants are associated with the passive oxide film response (R1–CPE1) and the charge-transfer process at the metal/electrolyte interface (R2–CPE2)

The EIS fitting results highlighted different passivation behaviors between bulk AA1099 and recycled-chip samples during immersion in NaCl solution. Bulk samples exhibited a strong increase in charge transfer resistance (R2) after 24 h, increasing from approximately 11.4 kΩ·cm² to 40.3 kΩ·cm², suggesting the formation of a highly protective passive film. Although R2 decreased after 72 h, it remained significantly higher than the initial value, suggesting that the passive layer retained substantial protective properties even after prolonged chloride exposure. Moreover, the increase of the n2 exponent toward values close to 1 further supports the development of a more homogeneous and ideal capacitive interface.

In contrast, recycled-chip samples showed a less stable electrochemical behavior. The increase in R2 after 24 h was limited, followed by a marked decrease after 72 h down to 5.4 kΩ·cm², indicating reduced stability of the passive layer in chloride-containing environment. The progressive decrease of n1 and the lower R1 values at longer immersion times point to increasing interfacial heterogeneity, consistent with the intrinsic microstructural features of the consolidated chips, such as residual oxide fragments, chip–chip interfaces and local defects generated during compaction and rolling. Overall, the EIS results suggest that recycled-chip samples develop a less protective and less stable passive film compared to bulk material, while still maintaining a moderate corrosion resistance in saline environment.

The present observations, however, are consistent with previous studies on solid-state recycled aluminum alloys, where improved or comparable corrosion resistance relative to conventionally processed material was reported. Taha et al. demonstrated that solid-state recycled aluminum alloys exhibit enhanced corrosion resistance compared to as-received material, which was attributed to the fragmentation and redistribution of surface oxides during severe plastic deformation, leading to a more protective and stable passive film in chloride-containing environments [33]. The present results are consistent with previous EIS studies on aluminum systems (e.g [34]., et al.), where the evolution of R2 and CPE parameters has been used to assess passive-film stability and interfacial heterogeneity. The decrease in R2 observed for recycled-chip samples after 72 h should therefore be interpreted as reduced passive-film stability rather than evidence of stable pitting corrosion.

Overall, the recycled aluminum chips exhibit corrosion behavior comparable to that of the bulk material under the investigated conditions. These results indicate that the direct hot rolling process does not adversely affect the corrosion performance of ultra-high purity aluminum, within the scope of the present experimental analysis.

4 Limitations of this study and industrial scale-up challenges

Despite the promising results obtained in this feasibility study, several limitations and industrial challenges must be acknowledged. The experiments were conducted using cleaned aluminum chips, whereas industrial machining chips often contain lubricants, oils, or other contaminants. Such residues may affect interfacial bonding during solid-state consolidation and would require appropriate preprocessing steps, such as degreasing or thermal cleaning, which may reduce process efficiency and overall sustainability and therefore require careful evaluation. For instance, it has been reported that a degreasing step can increase the overall environmental impact (expressed in terms of single-score

Table 5 Electrochemical impedance spectroscopy (EIS) fitting parameters obtained for bulk AA1099 and recycled-chip samples after immersion in 35 g/L NaCl solution for 0, 24 and 72 h

	Unit	Bulk t0	Bulk t24	Bulk t72	Chips t0	Chips t24	Chips t72
Rs	Ω cm²	10.16	19.20	18.51	13.35	23.23	81.98
Q1	μS s^n cm^{-2}	36.97	30.17	32.78	33.65	22.71	18.83
n1	—	0.92	0.85	0.85	0.87	0.89	0.74
R1	Ω cm²	12,737	15,062	13,088	17,004	10,897	10,502
CPE1	μF cm^{-2}	34.71	26.29	28.13	30.89	18.96	10.70
Q2	mS s^n cm^{-2}	0.42	5.24	4.77	3.46	6.18	0.0155
n2	—	0.68	1.00	0.94	1.00	1.00	0.93
R2	Ω cm²	11,396	40,279	21,278	8,580	9,836	5,410
CPE2	mF cm^{-2}	0.86	5.24	6.27	3.46	6.18	0.0129

impact points) of solid-state recycling processes by more than 20%, highlighting a critical trade-off between final material quality and overall process sustainability [35, 36].

Another important limitation concerns the use of ultra-high purity aluminum (AA1099), which differs significantly from industrial aluminum swarf that typically contains alloying elements such as Mg, Cu, and Zn. These elements can strongly affect recrystallization kinetics, oxide fragmentation, precipitate pinning, and interfacial bonding during solid-state consolidation. Therefore, the present results should be interpreted as a fundamental feasibility assessment of the DHR process under controlled metallurgical conditions rather than a direct representation of industrial recycling scenarios.

The chip-derived sheets exhibited jagged and sawtooth-like edges after multi-pass rolling, leading to material losses during trimming. While edge trimming is a standard and unavoidable operation even in conventional industrial rolling processes, optimizing the initial chip compaction geometry may be necessary to improve edge quality, processing efficiency, and minimizing scrap generation.

From an industrial perspective, the direct hot rolling route for chips relies on conventional rolling equipment and does not require melting furnaces, offering potential advantages in terms of energy consumption and CO_2 emissions. Nevertheless, a full quantitative life cycle assessment, including a direct comparison of energy consumption per ton of aluminum with conventional remelting-based recycling routes, was beyond the scope of the present work. Although existing literature suggests substantial energy savings from eliminating melting, a detailed techno-economic and life cycle assessment (accounting for all preprocessing, heating, and rolling operations) is essential to accurately evaluate the feasibility of large-scale implementation.

5 Conclusions

This work demonstrates the fundamental feasibility of direct hot rolling as a solid-state recycling route for pure AA1099 aluminum chips under controlled and uncontaminated laboratory conditions. The results should be interpreted as a mechanism-verification study rather than as direct evidence of immediate industrial applicability to mixed or contaminated aluminum machining chips. Extension of this approach to industrial-grade chip recycling will require further investigation involving alloyed aluminum systems, contaminated chips, lubricant removal, oxide control, and process scale-up. The main findings are:

1. The recycled chip-based sheets achieved average mechanical properties close to the bulk-processed counterpart, although a higher scatter was observed, highlighting the influence of microstructural heterogeneities and localized interfacial bonding typical of chip-based solid-state recycling.
2. Optical/EBSD analyses confirmed successful consolidation without macroscopic cracking or large voids at the examined scale, while revealing a layered/elongated morphology in the chip-based material consistent with thermomechanical bonding of fragmented chips.
3. FE-SEM/EDS observations identified localized sub-micrometric interfacial discontinuities with oxygen enrichment, indicating that residual oxide at prior chip boundaries can persist in limited regions despite overall effective bonding.
4. Potentiodynamic polarization in 3.5 wt% NaCl showed corrosion parameters for the recycled material comparable to bulk AA1099, indicating that the direct hot rolling process does not adversely affect the corrosion performance of ultra-high purity aluminum under the investigated conditions. EIS analysis further revealed that, although bulk AA1099 developed a more stable passive response during immersion, recycled-chip samples maintained moderate corrosion resistance, with the lower stability after 72 h likely related to interfacial heterogeneity, residual oxide fragments and chip–chip bonding regions.

Despite these promising results, several challenges remain. The jagged edges produced during rolling of the chip-derived samples introduce additional material loss, which necessitates optimization of the initial chip compaction geometry to enhance processing efficiency. Moreover, in this study, the aluminum chips were cleaned before processing, whereas in industrial settings, chips contain contaminants such as lubricants, which could affect the final material properties. Future work should therefore focus on refining the pretreatment steps and a comprehensive industrial feasibility analysis. Extension of this approach to industrial-grade chip recycling will require further investigation involving alloyed aluminum systems, contaminated chips, lubricant removal, oxide control, and process scale-up. Future developments should also focus on building a dedicated quantitative oxide-fragmentation model for direct hot rolling, combining TEM-based statistical analysis, oxygen-content measurements, and surface-sensitive characterization techniques to correlate oxide morphology, interfacial bonding, grain-boundary pinning, and final mechanical properties.

Funding Open access funding provided by Università degli Studi di Cagliari within the CRUI-CARE Agreement. No funding was received to assist with the preparation of this manuscript.

Declarations

Competing interests The authors have no competing interests to declare that are relevant to the content of this article.

References

1. Raabe D, Ponge D, Uggowitzer PJ, Roscher M, Paolantonio M, Liu C, Antrekowitsch H, Kozeschnik E, Seidmann D, Gault B et al (2022) Making sustainable Aluminum by recycling scrap: The science of "dirty" alloys. Prog Mater Sci 128:100947. https://doi.org/10.1016/j.pmatsci.2022.100947
2. Laurent-Brocq M, Lilensten L, Pinot C, Schulze A, Duchaussoy A, Bourgon J, Leroy E, Tekkaya AE (2023) Solid state recycling of aluminium chips: multi-technique characterization and analysis of oxidation. Materialia 101864. https://doi.org/10.1016/j.mtla.2023.101864
3. Al-Alimi S, Lajis MA, Shamsudin S, Yusuf NK, Chan BL, Hissein DD, Rady MH, Msebawi MS, Sabbar HM (2021) Hot Extrusion Followed By A Hot ECAP Consolidation Combined Technique In The Production Of Boron Carbide (B4C) Reinforced With Aluminium Chips (AA6061) Composite. Mater Tehnol 55. https://doi.org/10.17222/mit.2020.177
4. Buffa G, Campanella D, Adnan M, La Commare U, Ingarao G, Fratini L (2024) Improving the Industrial Efficiency of Recycling Aluminum Alloy Chips Using Friction Stir Extrusion: Thin Wires Production Process. Int J Precis Eng Manuf -Green Tech. https://doi.org/10.1007/s40684-023-00573-w
5. Puleo R, Latif A, Ingarao G, Fratini LA (2024) Generalized Parametric Model for the Bonding Occurrence Prediction in Friction Stir Consolidation of Aluminum Alloys Chips. J Manuf Process 131:604–618. https://doi.org/10.1016/j.jmapro.2024.09.049
6. Paraskevas D, Vanmeensel K, Vleugels J, Dewulf W, Deng Y, Duflou J (2014) Spark Plasma Sintering As a Solid-State Recycling Technique: The Case of Aluminum Alloy Scrap Consolidation. Materials 7:5664–5687. https://doi.org/10.3390/ma7085664
7. Paraskevas D, Kellens K, Deng Y, Dewulf W, Kampen C, Duflou JR (2017) Solid State Recycling of Aluminium Alloys via a Porthole Die Hot Extrusion Process: Scaling up to Production. AIP Conf Proc 1896:140008. https://doi.org/10.1063/1.5008164
8. El Mehtedi M, Buonadonna P, El Mohtadi R, Loi G, Aymerich F, Ben Khalifa N, Carta M (2024) Feasibility study of solid-state recycling through direct hot rolling of AA5754 aluminum chips for automotive applications. MSF 1130:3–12. https://doi.org/10.4028/p-J0bRTh
9. Carta M, Ben Khalifa N, Buonadonna P, Mele A, El Mehtedi M (2024) Life Cycle Assessment (LCA) of a Novel Solid-State Recycling Process for Aluminum Alloy AA6063 Chips via Direct Hot Rolling.; ; Vol. 41, pp. 2881–2890
10. El Mehtedi M, Buonadonna P, Carta M, El Mohtadi R, Mele A, Morea D (2023) Sustainability study of a new solid-state Aluminum chips recycling process: A Life Cycle Assessment approach. Sustainability Basel 15:11434. https://doi.org/10.3390/su151411434
11. El Mehtedi M, Carta M, Buonadonna P (2025) A novel Direct Hot Rolling Process for sustainable recycling of AA3105 Aluminum chips using a protective envelopment. Manuf Lett 45:70–74. https://doi.org/10.1016/j.mfglet.2025.06.208
12. Carta M, Ben Khalifa N, Buonadonna P, Aymerich F, El Mehtedi M (2025) Solid-State recycling of AA6063 Aluminum chips via Accumulative Roll Bonding: A green pathway to high-performance materials. Metals Basel 15:1042. https://doi.org/10.3390/met15091042
13. Anas NS, Ramteke KN, Kumar RA, Chouhan RN, Agnihotri A (2023) Effect of Compaction Pressure on Cold Compaction of AA2024 Swarf Generated during Milling Operation. *Materials Today: Proceedings* https://doi.org/10.1016/j.matpr.2023.09.106
14. Mohammed A-J, Maher I, Nakai M, Gepreel MAH (2023) Effects of Cold Rolling and Heat Treatment on the Microstructure and Hardness of Pure Aluminium. *Materials Today: Proceedings* S2214785323048101. https://doi.org/10.1016/j.matpr.2023.09.138
15. Humphreys FJ, Hatherly M (2004) *Recrystallization and Related Annealing Phenomena*; ; ISBN 978-0-08-044164-1
16. Chen S, Zou G, Xu Y, Li J, Duan T, Liu Y, Ye L (2025) Effect of Rolling Schedule on Grain Refinement and Superplasticity of 7475 Al–Zn–Mg–Cu Alloy Sheet. J Mater Res Technol 39:9465–9476. https://doi.org/10.1016/j.jmrt.2025.11.192
17. Szota P, Mróz S, Gontarz A, Stefanik A (2019) Theoretical and Experimental Analysis of Mg/Al Bimetallic Handle Forging Process. Arch Metall Mater 1503–1512. https://doi.org/10.24425/amm.2019.130119
18. Tomesani L (2008) Esercitazioni Di Lavorazioni per Deformazione Plastica. Società editrice Esculapio, Bologna (IT)
19. Cappai L, Casu M, Locci AM, Cao G, Garroni S, Cannillo V, Bellucci D, Orrù R (2025) From individual to equimolar binary transition metal diborides: the case of (Nb0.5M0.5)B2, M = Ti, Hf. J Eur Ceram Soc 45:117277. https://doi.org/10.1016/j.jeurceramsoc.2025.117277
20. Lv Y-Y, Zhang L-F, Wang G-X, Xiong Y (2017) Effect of Rolling and Annealing on Microstructure and Mechanical Properties of High Purity Aluminum. In Proceedings of the Proceedings of the 3rd Annual International Conference on Advanced Material Engineering (AME 2017); Atlantis Press: Shanghai, China
21. Zhang Z, Liang J, Xia T, Xie Y, Chan SLI, Wang J, Zhang D (2023) Effects of oxide fragments on microstructure and mechanical properties of AA6061 Aluminum alloy tube fabricated by thermomechanical consolidation of machining chips. Materials 16:1384. https://doi.org/10.3390/ma16041384
22. Bate P (2001) The Effect of Deformation on Grain Growth in Zener Pinned Systems. Acta Mater 49:1453–1461. https://doi.org/10.1016/S1359-6454(01)00033-7
23. Gao Q, Wang X, Li J, Gong J, Li B (2021) Effect of Aluminum on Secondary Recrystallization Texture and Magnetic Properties of Grain-Oriented Silicon Steel. J Iron Steel Res Int 28:479–487. https://doi.org/10.1007/s42243-020-00517-7
24. Duchateau T, Lilensten L, Zhang X, Gebhard J, Tekkaya AE, Laurent-Brocq M (2025) Effect of annealing on oxidation during solid-state recycling of Aluminium chips. J Alloys Compd 1010:178178. https://doi.org/10.1016/j.jallcom.2024.178178
25. Mondolfo LF (1979) *Aluminium Alloys: Structure and Properties*; Repr.; Butterworths: London, ; ISBN 978-0-408-70932-3
26. Gu J-D, Ford T, Mitchell R (2011) Uhlig's Corrosion Handbook, Third Edition. In; ; pp. 549–557 ISBN 978-0-470-08032-0
27. Munir S, Pelletier MH, Walsh WR (2016) Potentiodynamic Corrosion Testing. JoVE 54351. https://doi.org/10.3791/54351
28. Sherif E-SM (2012) Effects of Exposure Time on the Anodic Dissolution of Monel-400 in Aerated Stagnant Sodium Chloride Solutions. J Solid State Electrochem 16:891–899. https://doi.org/10.1007/s10008-011-1438-0
29. ACM Instruments (2000) Version 4 Operation Guide - ACM Instruments

30. Badawy WA, Al-Kharafi FM, El-Azab AS (1999) Electrochemical Behaviour and Corrosion Inhibition of Al, Al-6061 and Al–Cu in Neutral Aqueous Solutions. Corros Sci 41:709–727. https://doi.org/10.1016/S0010-938X(98)00145-0
31. Sherif EM, Park S-M (2005) Effects of 1,5-Naphthalenediol on aluminum corrosion as a corrosion inhibitor in 0.50 M NaCl. J Electrochem Soc 152:B205. https://doi.org/10.1149/1.1914752
32. Totten GE, MacKenzie DS (2003) *Handbook of Aluminum: Volume 2: Alloy Production and Materials Manufacturing*; CRC Press, ; ISBN 978-0-8247-4843-2
33. Taha MA, Abbas AT, Benyahia F, Alharbi HF, Guitián B, Nóvoa XR (2019) Enhanced corrosion resistance of recycled Aluminum Alloy 6061 chips using hot extrusion followed by ECAP. J Chem 2019:1–8. https://doi.org/10.1155/2019/3658507
34. Yasakau KA, Starykevich M, Ferreira MGS, Zheludkevich ML (2021) A critical look at interpretation of electrochemical impedance spectra of sol-gel coated aluminium. Electrochim Acta 378:138091. https://doi.org/10.1016/j.electacta.2021.138091
35. Duflou JR, Tekkaya AE, Haase M, Welo T, Vanmeensel K, Kellens K, Dewulf W, Paraskevas D (2015) Environmental Assessment of Solid State Recycling Routes for Aluminium Alloys: Can Solid State Processes Significantly Reduce the Environmental Impact of Aluminium Recycling? CIRP Ann 64:37–40. https://doi.org/10.1016/j.cirp.2015.04.051
36. Carta M, Buonadonna P, El Mohtadi R, Lai D, El Mehtedi M (2025) Evaluation of the Environmental Impact of Direct Hot Rolling, ECAP and FSE for Aluminum Chips Recycling.; ; pp. 2556–2565